Understanding Capacitance Variation in Sub-Nanometer Pores by *In-Situ* Tuning of Interlayer Constrictions

Dona T. L. Galhena[1], *Bernhard C. Bayer*[1,2], *Stephan Hofmann*[1], *Gehan A. J. Amaratunga*[1,3*]

[1] Electrical Engineering Division, Department of Engineering, University of Cambridge, 9 J. J. Thomson Ave., CB3 0FA, Cambridge, UK.

[2] Faculty of Physics, University of Vienna, Boltzmanngasse 5, A 1090 Vienna, Austria.

[3] Sri Lanka Institute of Nanotechnology (SLINTEC), Pitipana, Homagama, Sri Lanka

*Corresponding author: gaja1@cam.ac.uk.

KEYWORDS: Electrical double-layer capacitors, Supercapacitors, Sub-nanometer Pores, Graphene oxide, Interlayer constrictions, *In-situ* X-ray diffractometry

ABSTRACT:

The contribution of sub-nanometer pores in carbon electrodes to the charge storage mechanism in supercapacitors has been the subject of intense debate for over a decade. Here we provide a model system based on graphene oxide, which employs interlayer

constrictions as a model for pore sizes that can be both controllably tuned and studied *in-situ* during supercapacitor device use. Correlating electrochemical performance and *in-situ* tuning of interlayer constrictions, we observe a peak in specific capacitance when interlayer constriction size reaches the diameters of unsolvated ions, supporting the hypothesized link between loss of ion solvation shell and anomalous capacitance increase for sub-nanometer pores.

Electrical double-layer capacitors (EDLCs), also called supercapacitors or ultracapacitors, are electrochemical devices which store energy through reversible adsorption of ionic species on electrode surfaces.[1] As a class of energy storage devices, which can also have high power density, supercapacitors comprised of carbonaceous[2,3] electrodes have attracted considerable attention and substantial efforts have been directed towards their enhancement *via* rational electrode material and electrolyte design. In particular, the control of the size and geometry of the nanopores in such highly porous carbon-based electrodes is an area of focus as the nanoporous structure strongly influences the power and energy densities which can be achieved. However, the understanding of the complex relationships between electrode pore sizes and the specific capacitance still remains limited and has been the subject of recent debate, in particular since an anomalous increase in specific capacitance was reported for carbon pore sizes less than 1 nanometer.[4–6] It has been argued that this anomalous increase in capacitance is linked to pore sizes which are smaller than the diameter of the solvated ions, leading to partial removal of the ion solvation shells and ion confinement effects upon ion adsorption into such sub-nanometer pores.[7–12] This hypothesized presence of *desolvated* ions in sub-nanometer pores and corresponding anomalous capacitance increase contrasts the hitherto accepted picture of *solvated* ion double-layer adsorption on electrode surfaces.[13] There remains however controversy about adsorption of ions into sub-nanometer pores, partly due to the difficulty of experimentally assessing the complex pore structure and surface area of common electrode materials[14,15] and partly due to the limited availability of direct *in-situ* insight into working supercapacitors.[16–22]

Here, we address both issues by introducing intercalation constrictions in a layered carbon electrode material as a model system for electrode pores, where the pore size analogue can be controlled and studied *in-situ* in an EDLC. The method employs facile and controlled propylene-carbonate (PC) driven[23] variations in the interlayer spacing of graphene oxide (GO) electrodes combined with *in-situ* X-ray diffractometry (XRD) and electrochemical capacitor testing to directly assess how the specific capacitance of the model electrodes scales with interlayer constriction size. This novel approach circumvents the debated use[14] of complex pore size distribution evaluations. Correlating electrochemical performance and *in-situ* interlayer constriction size determination, we indeed observe a peak in specific capacitance when the interlayer constriction size reaches the diameters of unsolvated ions. The result we report experimentally supports the hypothesized link between loss of ion solvation shell and the anomalous capacitance increase.[7–12]

Results and Discussion

Free-standing, flexible and binder-free GO paper[24–26] was synthesized using graphite oxide derived from vein graphite following Hummer's method.[27] As produced GO paper was characterized using different complementary methods before assembly into an EDLC (see also Supplementary Text). The results clearly confirmed complete oxidation of the initial graphite to GO and successful fabrication of GO paper (see also Supplementary Text) consisting of densely and homogeneously turbostratically re-stacked GO sheets (Supporting Fig. S1), decorated with hydroxyl, carbonyl, ether and carboxyl groups, keeping an interlayer distance of ~0.82 nm (Supporting Fig. S2).

To assess the electrochemical behavior of GO, completely dried GO paper was used as the electrode material in a symmetric two-electrode EDLC device with tetraethylammonium tetrafluoroborate ($TEABF_4$) dissolved in propylene-carbonate (PC) as the electrolyte. The initial cyclic voltammetry (CV) measurements gave a specific capacitance of 0.13 F/g at a scan rate of 100 mV/s. From electrochemical impedance spectroscopy (EIS), the initial equivalent series resistance (ESR) was measured to be 28.6 Ω (Supporting Fig. S3). After the initial measurements, the GO paper device was electrochemically cycled between 0 V to +1 V at a scan rate of 100 mV/s up to 100,000 cycles (the comparably high scan rate was chosen to avoid unacceptably long experimental acquisition times), where EIS measurements were done after every 4,000 cycles. Concurrently, electrochemical results are correlated with *in-situ* XRD measurements (X-ray wavelength: 1.5406 Å) on the working device after defined numbers of electrochemical cycles to examine the effect of cycling on the variation in layer spacing in the GO electrodes.

The change in raw CV curve shapes with continuous electrochemical cycling of the capacitor within the narrow voltage range from 0 V to +1 V is shown in Fig. 1a, where the change in extracted specific capacitance of the EDLC with cycle number is shown in Fig.1b. (See Supporting Fig. S3 for the corresponding EIS results.)

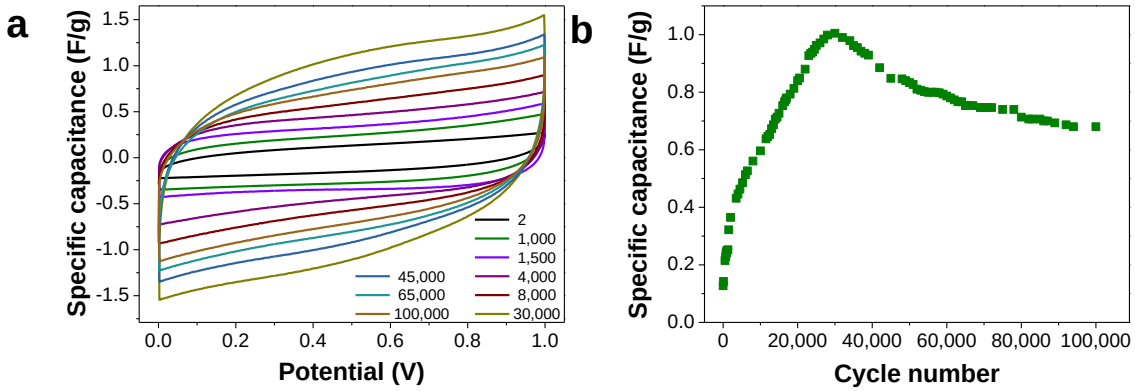

Figure 1: Electrochemical performance of the EDLC with GO paper electrodes in $TEABF_4$ electrolyte dissolved in PC. (**a**) CV curves recorded at different cycle numbers, in the voltage range 0 V to +1 V at 100 mV/s scan rate. (**b**) Variation in specific capacitance with cycle number. Relative uncertainty in extracted specific capacitance is estimated to 10%.

The electrochemical cycling revealed that the specific capacitance of the device initially increased gradually (from 0.13 F/g) with cycle number and then reached a maximum of 1.00 F/g at ~30,000 cycles. Subsequently the capacitance started to decrease gradually to reach 0.68 F/g after 100,000 cycles (at the end of experiment).

The variation in the interlayer distance of the GO electrodes within the working device was monitored by *in-situ* XRD measurements at selected cycle numbers (Fig. 2) and thus correlated to changes in the electrochemical performance of the model supercapacitor electrodes. After defined numbers of cycles, without disassembling the device, XRD measurements were taken on GO electrodes of the EDLC after sweeping the bias to 0 V and disconnecting from the voltage supply. XRD patterns of both electrodes were recorded (*via* flipping the coin cell), whereby both electrodes were observed to show similar changes in the XRD patterns and interlayer distances with cycling (Supporting Table S1). Therefore, the XRD patterns recorded in Fig. 2 are considered to be representative for the state of both GO electrodes (positive electrode and the negative electrode) (see also Supplementary Text).

For the as fabricated device (*i.e.* before any electrochemical cycling) a dominant XRD peak at 2θ = ~10.7°is observed (Fig. 2), consistent with the GO average interlayer distance of ~0.82 nm in the as prepared GO paper (Supporting Fig. S2a). With increasing cycle numbers, a clear shift of this peak to lower 2θ values is seen, indicating an expansion of the GO average interlayer distance with cycling. After 100,000 cycles a 2θ = ~5.3° is measured. This corresponds to a ~1.65 nm average interlayer distance. Such a shift clearly indicates an increase in the average interlayer spacing of the GO electrode with electrochemical cycling. The narrow bias range (from 0 to +1 V) allows gradual PC-driven exfoliation[23] of the GO electrode in the working capacitor, thus gradually increasing the GO average interlayer distance, but prevents adverse side reactions such as electrochemical reduction of GO[28–32] and redox-driven intercalation of electrolyte ions[33–38] with cycling,

ensuring that the GO nature of the electrodes is indeed maintained throughout the electrochemical cycling (see also Supplementary Text).

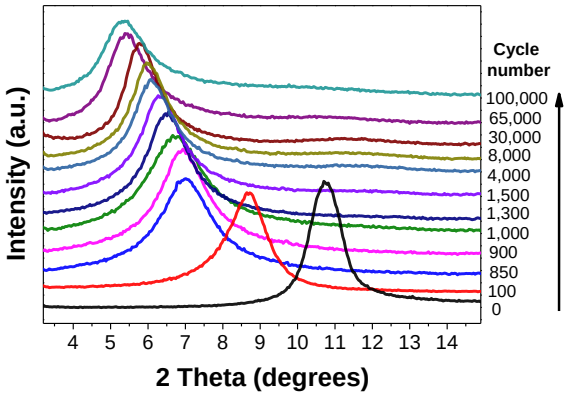

Figure 2: Electrochemical *in-situ* x-ray diffraction study of the EDLC device with GO electrodes in $TEABF_4$ electrolyte dissolved in PC. XRD scans (X-ray wavelength: 1.5406 Å) were collected on the GO electrodes of the EDLC after certain numbers of cycles to examine the effect of electrochemical cycling on the variation in layer spacing in the GO electrodes.

To further analyze the XRD data, the *increment* in GO average layer spacing (Δd) with cycle number is given in Fig. 3a. The increment in average interlayer distance (Δd) is equivalent to the average interlayer constriction size in the layered electrode material. It should be noted that the increment in GO average layer spacing/average interlayer constriction size (Δd) was calculated by considering the initial average spacing of the GO

layers (before any electrochemical cycling) as the zero point. Therefore, the increment in average layer spacing (Δd) after an n number of cycles can be given as:

$$\Delta d = d_n - d_0$$

with, d_n = (002) average interlayer distance between two GO layers after a n number of cycles

d_0 = (002) average interlayer distance between two GO layers of as synthesized GO (0.82 nm)

As seen in Fig. 3a, Δd follows a sharp increase at the beginning, up to about 1,500 cycles and then continues to further increase until the end of the experiment, but at a lower rate. Variation of the capacitance with cycle number (Fig. 1b) is also given again on the same plot for comparison. By re-plotting this data in Fig. 3b in the form of specific capacitance *against* the increment in average GO layer spacing (Δd) it can be seen how specific capacitance and average layer spacing increase are correlated and the key finding is revealed: Initially the specific capacitance increases gradually from 0.13 F/g to 0.32 F/g as the Δd increases from 0 to ~ 0.60 nm, then there is a sharp peak in specific capacitance rising up to 1.00 F/g as the Δd reaches to 0.70 nm. Then as the Δd further increases beyond 0.70 nm, the specific capacitance again sharply decreases and reaches a value of 0.68 F/g at Δd = 0.83 nm at the end of the experiment. This demonstrates a very direct correlation of a specific capacitance increase and average interlayer constriction size in the GO electrodes.

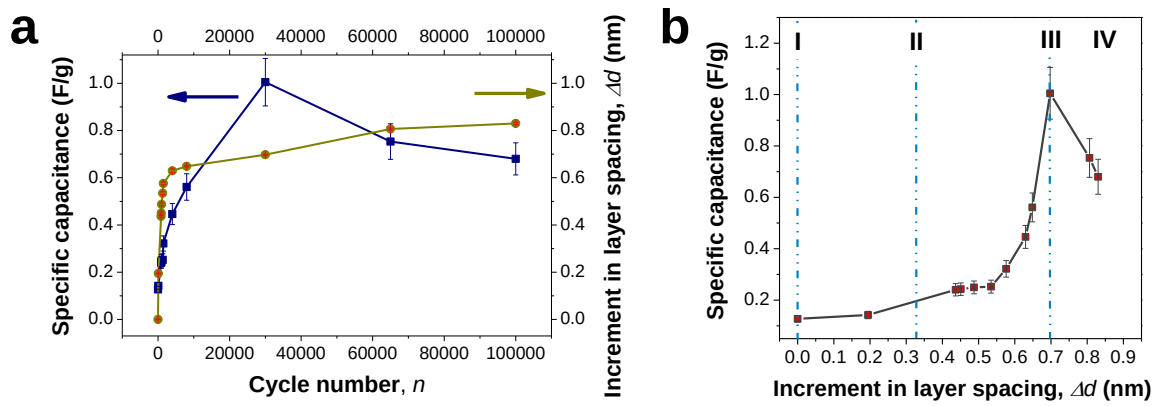

Figure 3: Correlation of increments in the average interlayer distance/interlayer constriction sizes (Δd) of the GO electrodes within the working EDLC to the variation of its electrochemical performance. (**a**) Specific capacitance and Δd, as a function of cycle number. (**b**) Variation of specific capacitance *versus* the increment in interlayer distance/interlayer constriction size Δd. Four stages, where Δd = 0 nm (I), 0.33nm (II) and 0.7 nm (III) and Δd >0.7 nm (IV), are indicated. Estimated uncertainty of the increments in the average interlayer distance/interlayer constriction sizes (Δd) are plotted in red for better legibility.

The key finding from Fig. 3b, that the average interlayer constriction size can be correlated with specific capacitance, can now be put into context of the prior literature on capacitance variation with pore size.

See Fig. 4 for a schematic illustration of GO layer spacing and how ions can intercalate as the spacing increases. Four main stages of interlayer distance variation indicated in Fig. 3b are schematically illustrated for both electrodes.

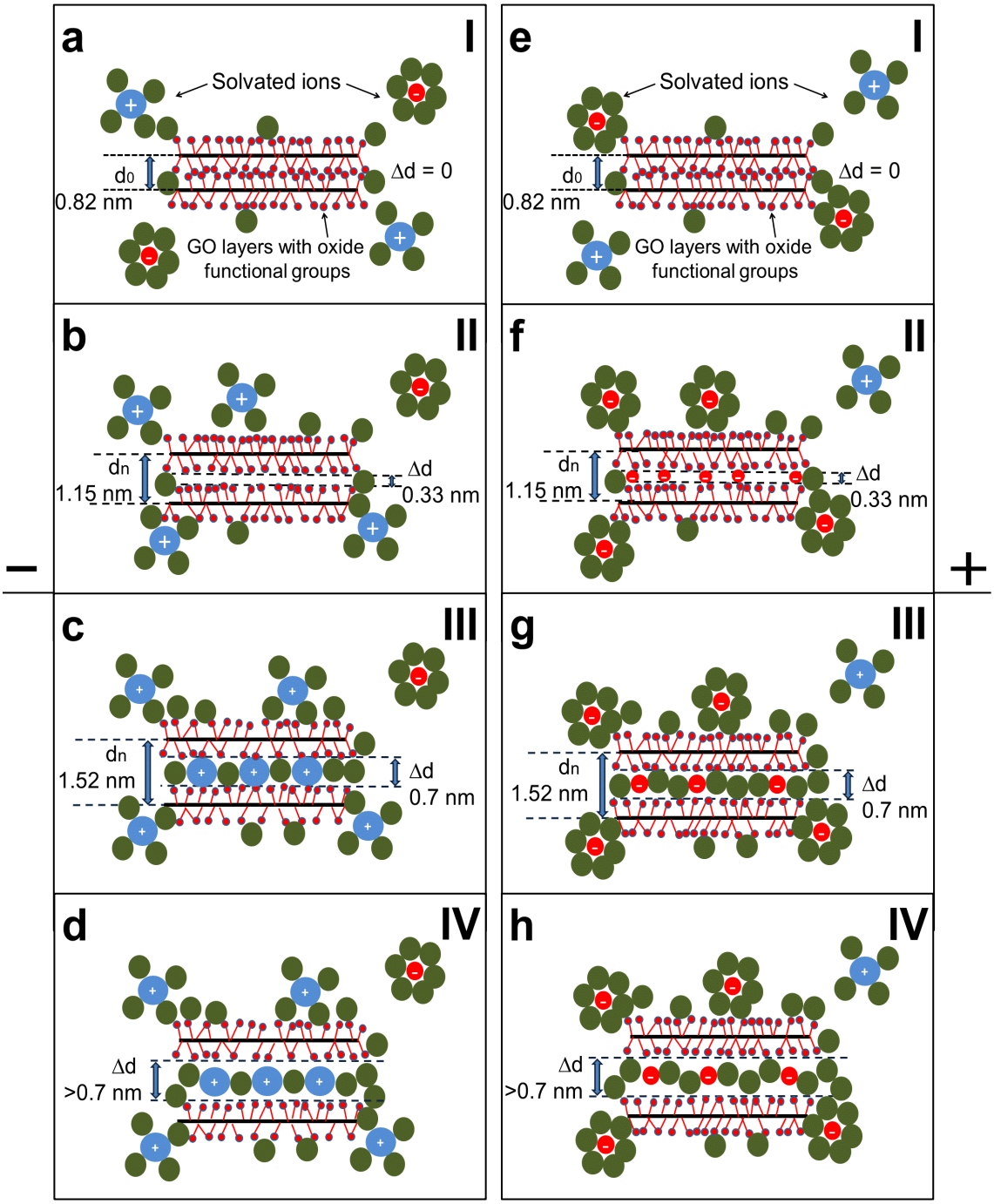

Figure 4: Schematic illustration of ion intercalation in GO layer spacing as interlayer constriction size increases in GO electrodes. Four stages of interlayer constriction size,

where Δd is 0 nm (I), 0.33 nm (II), 0.7 nm (III) and Δd >0.7 nm (IV) are illustrated for the negative electrode (**a-d**) and for the positive electrode (**e-h**).

The sizes of the various molecules and ions involved in the processes are as follows. Electrolyte solvent propylene carbonate (PC) has a molecule size of 0.61 nm.[39] The smaller BF_4^- ions has an unsolvated ion size of 0.33 nm,[5] which increases to 1.71 nm when BF_4^- is immersed in a PC solvation shell.[39] The larger TEA^+ ion has a size of 0.68 nm in its unsolvated state,[5] which increased to 1.96 nm when fully solvated.[39]

First, at the first stage of average interlayer spacing variation, the average interlayer constriction size, Δd, corresponds to 0.0 nm. In the as fabricated EDLC devices (*i.e.* before any cycling) the re-stacked GO electrodes show the typical GO equilibrium layer spacing[23] of 0.82 nm (Δd=0). This layer spacing is caused by the space requirements of the various oxide groups on the GO basal planes.[40] Therefore electrolyte ion intercalation is fully constricted by the closely packed re-stacked GO layers. Consequently the specific capacitance of the supercapacitor shows its lowest value.

Secondly, as the electrochemical cycling continues, the interlayer spacing progresses into the second stage where average interlayer constriction size Δd increases from 0.0 to 0.6 nm. With cycling, the electrolyte solvent propylene carbonate (PC, molecule size 0.61 nm)[39] aids the gradual increase of average interlayer distance in GO and the electrodes' interlayer constriction size starts to increase. This is consistent with previously reported facile GO exfoliation in PC.[23] The intrinsic propensity of PC molecules

to promote GO exfoliation combined with the applied voltage sweep from 0V to +1V leads to PC molecules "wedging" between the GO layers in increasing amounts. Here the increment in average layer spacing is driven by the solvent PC[23] and consequently the average layer spacing increases equally in both electrodes, as observed in our XRD data (Supporting Table S1).

In Fig. 3a, it can be observed that the increase in average layer spacing/interlayer constriction size (Δd) follows a sharp increase at the beginning (up to about 1,500 cycles) from 0 to ~ 0.60 nm. However, the specific capacitance in this constriction size range shows only a gradual increase from 0.11 F/g to 0.32 F/g. The sharp increase in Δd, which does not result in a sharp increase in capacitance, can be attributed to the comparatively rapid intercalation of solvent PC molecules between GO planes at the beginning of the cycling experiment. Initially, neither BF_4^- nor TEA^+ can intercalate through the GO interlayer constrictions in this region even after shedding their solvation shell. After a number of cycles, the Δd becomes large enough for completely or partially desolvated smaller BF_4^- ions to absorb into the GO interlayer space of the positive electrode (un-solvated BF_4^- ion size = 0.33 nm).[5] With repeated cycling, the positive electrode starts to become increasingly accessible to completely or partially desolvated BF_4^- ions. With Δd between 0.33 nm and 0.6 nm, the capacitance of the whole symmetric supercapacitor device (*i.e.* two capacitors in series) is however still limited by the capacitance at the negative electrode because TEA^+ ions are still too large to pass through the GO intercalation constrictions. Thus the capacitance of the device is dependent on the accessibility of TEA^+ ions into the GO electrode interlayer spaces. At this stage, upon

removal of the applied bias, to maintain the charge neutrality, TEA^+ ions cannot move in to the interlayer spacings of the positive electrode due to the size restrictions. Therefore, we speculate that BF_4^- ions move out from the apertures. Since the increment in layer spacing is driven by the neutral solvent PC molecules, but not the ions intercalated between the layers, the interlayer spacing will not be changed as the BF_4^- ions move out from the positive electrode.

In the third stage, when a GO interlayer constriction size of Δd = ~0.70 nm is approached, a drastic increase in specific capacitance occurs. With opening of the intercalation constrictions to be large enough for the un-solvated larger TEA^+ ions (0.68 nm) to be adsorbed on the GO surface plane, the negative electrode can take up a significantly increased amount of TEA^+ ions. At this point, both the positive electrode and the negative electrode become completely accessible to their respective ions; positive electrode to the completely or partially desolvated BF_4^- ions and negative electrode to the comparably larger desolvated TEA^+ ions. Consequently, a strong increase in the total capacitance of the whole EDLC occurs for Δd from 0.6 nm to 0.7 nm, as observed in Fig. 3b.

We note that the increase in GO interlayer distance is irreversible as it is not driven by electrolyte ion intercalation but by gradual “wedging in” of solvent PC molecules. Thus when the supercapacitor is discharged, the space between GO layers remains occupied by electrolyte species, with an equal proportion of cations and anions, as evidenced by a recent NMR study.[16] This allows the accurate measurement of the layer spacing of the GO electrodes after ion intercalation although the device is measured in the discharged state.

Since the increment in layer spacing is driven by the solvent PC (but not the ions), it continues to increase even after both ions can pass the intercalation constrictions and fully access the GO interlayer space and reaches the fourth stage where $\Delta d > 0.7$ nm. When the average interlayer constriction size further increases, but still stays below the size of fully solvated BF_4^- and TEA^+ ions, interestingly the capacitance again starts to decrease sharply. This is attributed to the increase in average distance between electrode layer and the center of the intercalated ions as well as to the relaxation in confinement of the desolvated ions.[6,8–12]

Contextualizing our results, we note that previous literature demonstrated a similar sharp peak behavior in specific capacitance for carbide derived carbon (CDC) electrodes as their pore size approached the size of the desolvated ions. In particular, Largeot *et al*. showed a strongly peaked capacitance between 0.65 and 0.8 nm CDC pore size in supercapacitors using ethyl-methylimmidazolium-bis(trifluoromethane-sulfonyl)imide ionic liquids (EMI-TFSI)[6] and Chmiola *et al*. showed a peaking behavior around 0.75 nm CDC pore size for TEA^+/BF_4^- supercapacitors using acetonitrile solvent.[4,5] Similar trends were observed in prior studies using activated carbons[41] and activated AR-resin-based carbons[39] and also using aqueous electrolytes.[42,43] All these results point to a different charge-storage mechanism than the hitherto commonly accepted double-layer formation of fully solvated ions. Instead, the partial removal of the solvation shell and the increased confinement of the ions when the pore sizes become smaller than the solvated ion radius have been proposed as the cause for increased capacitance. A number of further

experimental[16,44–48] as well as theoretical and modelling studies[7–12] have attempted to provide insights into this hypothesis.

On the other hand, Centeno *et al.*[14] have reported in a recent study of 28 porous carbons, that they found the specific capacitance in the electrolyte $(C_2H_5)_4NBF_4$/acetonitrile to be relatively constant between 0.7 and 15 nm. There, contrary to the studies cited above, the specific capacitance increase in pores below 1 nm was not observed at all but the previous results were rather attributed to misleading interpretation of surface area measurements.[14,15] This makes the issue of capacitance enhancement in sub-1-nm pores still controversial.

A fundamental reason for this controversy is that the control and accurate experimental determination of the pore size distribution is difficult for common complex carbon-based electrode materials. Our approach of controllably investigating the pore size dependence of specific capacitance by using *in-situ* tunable interlayer constrictions in layered electrode materials (here shown for GO) as a model for pore sizes is aimed to fill this gap. As discussed above our results strongly point towards support of the hypothesis of an anomalous capacitance increase linked to pore sizes around the size of the unsolvated ions.

Conclusions

In conclusion, we present a new approach to address the long-held controversy on contribution of sub-nanometer pores of carbon electrodes to the charge storage in EDLCs by introducing a model system based on GO. This employs interlayer constrictions of GO as a model for pore sizes that can be both controllably tuned and studied *in-situ* during

supercapacitor device use. Polar surface oxide groups make GO electrically insulating[40] and could impact on electrolyte ion uptake dynamics. Therefore GO is normally not a preferred electrode material for supercapacitors in application scenarios.[49,50] While this naturally leads to low absolute specific capacitance values for the GO electrodes in our study, as a model system, binder-free GO paper electrodes uniquely allow controllable and facile (here PC-driven) exfoliation of its layered structure and thus a gradual increase in interlayer constriction size. The interlayer spacings are measurable through XRD obtained *in-situ*. It is thereby possible to assess the correlation of interlayer spacing and relative change in specific capacitance, as shown here. Taking increase in average interlayer spacing as a proxy for constriction size in porous materials, the GO electrodes combined with our *in-situ* approach are therefore an effective first-order-approximation model system to study the variation of capacitance in ultra-small pores. Our methodology of *in-situ* XRD and electrochemical cycling combined with controllable tuning of interlayer spacing is extendable to other layered materials (such as reduced GO (r-GO), graphite, transition metal dichalcogenides *etc*.), albeit, as controlled solvent driven exfoliation of these (compared to GO) more strongly bound layered materials is more challenging. Future work needs to deal with changes in solvent chemistry or larger electrochemical cycling windows in order to allow similarly facile and controlled solvent driven exfoliation and thus associated controlled changes in interlayer constriction size. In doing so, the approach has potential application, not only in the energy storage area (supercapacitors) but more generally in any field dealing with ion transport through nano-pores such as water desalination or the function of ion channels in cells.

Methods

Synthesis of GO paper

Graphite oxide was synthesized from natural vein graphite (purity >99%, Bogala Graphite, Sri Lanka) by Hummers method as originally presented by Hummers and Offeman.[27] As-synthesized graphite oxide was washed with a diluted HCl solution to completely remove residual salts. It was further washed with water until the pH of the rinse water becomes neutral (pH = 7). Ultrapure Milli-Q® water was used in all experiments. As purified graphite oxide suspensions were then dispersed in water. Exfoliation of graphite oxide to GO was achieved by ultra-sonication of the dispersion. Graphene oxide dispersions prepared according to the above procedure were dried slowly in an oven maintained at a temperature of 50 °C, to obtain a film of graphene oxide attached to the substrate.[24,25] This GO paper consists of GO layers which settled and turbostratically re-stacked from their dispersed state in solution upon drying of the paper. Completely dried, GO paper was then carefully peeled from its substrate and used for further characterization and electrical double-layer capacitor (EDLC) fabrication. See Supporting Information for additional characterization of the GO electrodes.

Electrochemical testing and in-situ materials characterization

The electrochemical behavior of the GO paper was characterized by cyclic voltammetry (CV) and electrochemical impedance spectroscopy (EIS) with two symmetric electrodes in coin cell geometry using an Autolab electrochemical interface instrument (PGSTAT 302N). Flat GO paper (~30 µm thickness) was used for electrodes as-is by cutting electrodes with an area of ~1.8 cm^2. A solution of 1M $TEABF_4$ (Sigma Aldrich) in PC (Sigma Aldrich) was used as the electrolyte and a filter paper (Waterman, grade no. 1, thickness ~180 µm) was used as the separator. Coin cell preparation was carried out in a nitrogen-filled glove box (M Braun) with oxygen and moisture levels of <1 ppm. Electrochemical measurements were taken using a two-electrode system at ambient temperature.

CV curves were recorded in the potential range from 0.0 to +1.0 V at 100 mV/s scan rate and the cycling behavior of the electrodes were characterized up to 100,000 cycles. Specific capacitance values as a function of cycle number were estimated through the current at 0.5 V or through raw data integration,[51] where both methods show good agreement and we estimate a relative uncertainty in stated specific

capacitance values of 10%. EIS measurements were performed over a frequency range from 0.1-100 kHz at amplitude of 10 mV at intervals of every 4,000 CV cycles. Extrapolating the curve on the Nyquist plot to intersect the X-axis yields equivalent series resistance (ESR) values.

To concurrently monitor the variation in the interlayer distance of GO electrodes within the EDLC, *in-situ* XRD measurements (Bruker D8, x-ray wavelength: 1.5406 Å) were carried out on the GO electrodes (information depth estimated to 50-200 µm, see Supplementary Text). After defined numbers of cycles, without disassembling the device, XRD measurements were taken on both electrodes of the EDLC after sweeping the bias to 0 V and disconnecting from the voltage supply. For this purpose, CR-2016 coin cell cases (EQ-CR2016-MTI), modified for *in-situ* XRD analysis of the electrode material, were used for EDLC fabrication. Both coin cell cases were modified to include 10 mm diameter Kapton windows of 25 µm thickness, to ensure maximum X-ray beam penetration. Both positive and negative electrode side were measured by XRD, showing good agreement and thus confirming homogeneous PC-driven layer expansion of both electrodes (see Supporting Information). XRD reflections were fitted by Gaussian profiles, where we state in the main text the extracted peak center values as the average interlayer spacing value *d*. Estimated uncertainty of the average interlayer spacing values is estimated to 3× computed fit uncertainty.

Cycling experiments have been conducted for several supercapacitor devices which were independently fabricated in different fabrication batches. We find a good reproducibility in the general trend of the key result of peaking behavior of specific capacitance when interlayer constriction size approaches the size of the unsolvated TEA^+ ion, confirming the generic nature of our findings to the studied electrode material.

Supporting Information Available:

Supplementary Text

Supplementary Figures S1 to S3

Supplementary Tables S1

Supplementary References

This material is available free of charge *via* the Internet at http://pubs.acs.org.

Author contributions

DTLG synthesized graphene oxide, designed and performed experiments, analyzed the data and wrote the first draft of the manuscript. BCB assisted with (*ex-situ*) material characterization, data interpretation, manuscript writing, and was involved in discussions on the electrochemical tests. SH and GAJA supervised the project. All authors discussed the results and commented on the manuscript.

Conflict of Interest: The authors declare no competing financial interest.

Acknowledgments:

DTLG acknowledges technical support by J. N. R. Grundy (University of Cambridge) and financial support from Newnham College, Cambridge and the Cambridge Commonwealth Trust. GAJA acknowledges partial support for this work from Dyson Ltd. BCB acknowledges a College Research Fellowship at Hughes Hall, Cambridge. DTLG and GAJA thank Ananda Hettiarachchy and K. M. N. de Silva for discussions on activated carbon.

References

(1) Simon, P.; Gogotsi, Y. Materials for Electrochemical Capacitors. *Nat. Mater.* **2008**, *7*, 845–854.

(2) Pandolfo, A. G.; Hollenkamp, A. F. Carbon Properties and Their Role in Supercapacitors. *J. Power Sources* **2006**, *157*, 11–27.

(3) Simon, P.; Gogotsi, Y. Capacitive Energy Storage in Nanostructured Carbon-Electrolyte System. *Acc. Chem. Res.* **2013**, *46*, 1094–1103.

(4) Chmiola, J.; Largeot, C.; Taberna, P. L.; Simon, P.; Gogotsi, Y. Desolvation of Ions in Subnanometer Pores and Its Effect on Capacitance and Double-Layer Theory. *Angew. Chem., Int. Ed.* **2008**, *47*, 3392–3395.

(5) Chmiola, J.; Yushin, G.; Gogotsi, Y.; Portet, C.; Simon, P.; Taberna, P. L. Anomalouse Increase in Carbon Capacitance at Pore Sizes Less Than 1 Nanomater. *Science* **2006**, *313*, 1760–1763.

(6) Largeot, C.; Portet, C.; Chmiola, J.; Taberna, P. L.; Gogotsi, Y.; Simon, P. Relation Between the Ion Size and Pore Size for an Electric Double-Layer Capacitor. *J. Am. Chem. Soc.* **2008**, *130*, 2730–2731.

(7) Kiyohara, K.; Sugino, T.; Asaka, K. Electrolytes in Porous Electrodes: Effects of the Pore Size and the Dielectric Constant of the Medium. *J. Chem. Phys.* **2010**, *132*, 144705.

(8) Feng, G.; Cummings, P. T. Supercapacitor Capacitance Exhibits Oscillatory Behavior as a Function of Nanopore Size. *J. Phys. Chem. Lett.* **2011**, *2*, 2859–2864.

(9) Xing, L.; Vatamanu, J.; Borodin, O.; Bedrov, D. On the Atomistic Nature of Capacitance Enhancement Generated by Ionic Liquid Electrolyte Confined in Subnanometer Pores. *J. Phys. Chem. Lett.* **2013**, *4*, 132–140.

(10) Kondrat, S.; Georgi, N.; Fedorov, M. V; Kornyshev, A. A. A Superionic State in Nano-Porous Double-Layer Capacitors: Insights from Monte Carlo Simulations. *Phys. Chem. Chem. Phys.* **2011**, *13*, 11359–11366.

(11) Kondrat, S.; Kornyshev, A. Superionic State in Double-Layer Capacitors with Nanoporous Electrodes. *J. Phys.: Condens. Matter* **2011**, *23*, 022201.

(12) Huang, J.; Sumpter, B. G.; Meunier, V. A Universal Model for Nanoporous Carbon Supercapacitors Applicable to Diverse Pore Regimes, Carbon Materials, and Electrolytes. *Chem. - Eur. J.* **2008**, *14*, 6614–6626.

(13) Conway, B. E. *Electrochemical Capacitors: Scientific Fundamentals and Technological Applications*; Kluwer Academic/ Plentium Publishers: New York, 1999.

(14) Centeno, T. A.; Sereda, O.; Stoeckli, F. Capacitance in Carbon Pores of 0.7 to 15nm:

A Regular Pattern. *Phys. Chem. Chem. Phys.* **2011**, *13*, 12403–12406.

(15) Centeno, T. A.; Stoeckli, F. The Volumetric Capacitance of Microporous Carbons in Organic Electrolyte. *Electrochem. Commun.* **2012**, *16*, 34–36.

(16) Deschamps, M.; Gilbert, E.; Azais, P.; Raymundo-Piñero, E.; Ammar, M. R.; Simon, P.; Massiot, D.; Béguin, F. Exploring Electrolyte Organization in Supercapacitor Electrodes with Solid-State NMR. *Nat. Mater.* **2013**, *12*, 351–358.

(17) Levi, M. D.; Salitra, G.; Levy, N.; Aurbach, D.; Maier, J. Application of a Quartz-Crystal Microbalance to Measure Ionic Fluxes in Microporous Carbons for Energy Storage. *Nat. Mater.* **2009**, *8*, 872–875.

(18) Wang, H.; Köster, T. K.-J.; Trease, N. M.; Ségalini, J.; Taberna, P.-L.; Simon, P.; Gogotsi, Y.; Grey, C. P. Real-Time NMR Studies of Electrochemical Double-Layer Capacitors. *J. Am. Chem. Soc.* **2011**, *133*, 19270–19273.

(19) Wang, H.; Forse, A. C.; Griffin, J. M.; Trease, N. M.; Trognko, L.; Taberna, P.-L.; Simon, P.; Grey, C. P. In Situ NMR Spectroscopy of Supercapacitors: Insight into the Charge Storage Mechanism. *J. Am. Chem. Soc.* **2013**, *135*, 18968–18980.

(20) Forse, A. C.; Griffin, J. M.; Wang, H.; Trease, N. M.; Presser, V.; Gogotsi, Y.; Simon, P.; Grey, C. P. Nuclear Magnetic Resonance Study of Ion Adsorption on Microporous Carbide-Derived Carbon. *Phys. Chem. Chem. Phys.* **2013**, *15*, 7722–7730.

(21) Bagge-Hansen, M.; Wood, B. C.; Ogitsu, T.; Willey, T. M.; Tran, I. C.; Wittstock, A.; Biener, M. M.; Merrill, M. D.; Worsley, M. A.; Otani, M.; Chuang, C.-H.; Prendergast, D.; Guo, J.; Baumann, T. F.; van Buuren, T.; Biener, J.; Lee, J. R. I. Potential-Induced Electronic Structure Changes in Supercapacitor Electrodes Observed by In Operando Soft X-Ray Spectroscopy. *Adv. Mater.* **2015**, *27*, 1512–1518.

(22) Richey, F. W.; Tran, C.; Kalra, V.; Elabd, Y. A. Ionic Liquid Dynamics in Nanoporous Carbon Nanofibers in Supercapacitors Measured with In Operando Infrared Spectroelectrochemistry. *J. Phys. Chem. C* **2014**, *118*, 21846–21855.

(23) Zhu, Y.; Stoller, M. D.; Cai, W.; Velamakanni, A.; Piner, R. D.; Chen, D.; Ruoff, R. S. Exfoliation of Graphite Oxide in Propylene Carbonate and Thermal Reduction of the Resulting Graphene Oxide Platelets. *ACS Nano* **2010**, *4*, 1227–1233.

(24) Dikin, D. A.; Stankovich, S.; Zimney, E. J.; Piner, R. D.; Dommett, G. H. B.; Evmenenko, G.; Nguyen, S. T.; Ruoff, R. S. Preparation and Characterization of Graphene Oxide Paper. *Nature* **2007**, *448*, 457–460.

(25) Kumarasinghe, A. R.; Samaranayake, L.; Bondino, F.; Magnano, E.; Kottegoda, N.; Carlino, E.; Ratnayake, U. N.; de Alwis, A. A. P.; Karunaratne, V.; Amaratunga, G. A. J. Self-Assembled Multilayer Graphene Oxide Membrane and Carbon Nanotubes Synthesized Using a Rare Form of Natural Graphite. *J. Phys. Chem. C* **2013**, *117*, 9507–9519.

(26) Hantel, M. M.; Kaspar, T.; Nesper, R.; Wokaun, A.; Kotz, R. Partially Reduced Graphene Oxide Paper: A Thin Film Electrode for Electrochemical Capacitors. *J. Electrochem. Soc.* **2013**, *160*, A747–A750.

(27) Hummers Jr., W. S.; Offeman, R. E. Preparation of Graphitic Oxide. *J. Am. Chem. Soc.* **1958**, *80*, 1339.

(28) Harima, Y.; Setodoi, S.; Imae, I.; Komaguchi, K.; Ooyama, Y.; Ohshita, J.; Mizota, H.; Yano, J. Electrochemical Reduction of Graphene Oxide in Organic Solvents. *Electrochim. Acta* **2011**, *56*, 5363–5368.

(29) Peng, X. Y.; Liu, X. X.; Diamond, D.; Lau, K. T. Synthesis of Electrochemically-Reduced Graphene Oxide Film with Controllable Size and Thickness and Its Use in Supercapacitor. *Carbon* **2011**, *49*, 3488–3496.

(30) Kauppila, J.; Kunnas, P.; Damlin, P.; Viinikanoja, A.; Kvarnström, C. Electrochemical Reduction of Graphene Oxide Films in Aqueous and Organic Solutions. *Electrochim. Acta* **2013**, *89*, 84–89.

(31) Ramesha, G. K.; Sampath, S. Electrochemical Reduction of Oriented Graphene Oxide Films: An In Situ Raman Spectroelectrochemical Study. *J. Phys. Chem. C* **2009**, *113*, 7985–7989.

(32) Shao, Y.; Wang, J.; Engelhard, M.; Wang, C.; Lin, Y. Facile and Controllable Electrochemical Reduction of Graphene Oxide and Its Applications. *J. Mater. Chem.* **2010**, *20*, 743–748.

(33) Hantel, M. M.; Kaspar, T.; Nesper, R.; Wokaun, A.; Kötz, R. Persistent Electrochemical Pillaring of Graphene Ensembles. *Electrochem. Commun.* **2013**, *34*, 189–191.

(34) Abdelkader, A. M.; Kinloch, I. A.; Dryfe, R. A. W. Continuous Electrochemical Exfoliation of Micrometer-Sized Graphene Using Synergistic Ion Intercalations and Organic Solvents. *ACS Appl. Mater. Interfaces* **2014**, *6*, 1632–1639.

(35) Ruch, P. W.; Hahn, M.; Rosciano, F.; Holzapfel, M.; Kaiser, H.; Scheifele, W.; Schmitt, B.; Novák, P.; Kötz, R.; Wokaun, A. In Situ X-Ray Diffraction of the Intercalation of $(C_2H_5)_4N^+$ and BF_4^- into Graphite from Acetonitrile and Propylene Carbonate Based Supercapacitor Electrolytes. *Electrochim. Acta* **2007**, *53*, 1074–1082.

(36) Campana, F. P.; Hahn, M.; Foelske, A.; Ruch, P.; Kötz, R.; Siegenthaler, H. Intercalation into and Film Formation on Pyrolytic Graphite in a Supercapacitor-Type Electrolyte $(C_2H_5)_4NBF_4$/Propylene Carbonate. *Electrochem. Commun.* **2006**, *8*, 1363–1368.

(37) Ruch, P. W.; Hahn, M.; Cericola, D.; Menzel, A.; Kötz, R.; Wokaun, A. A Dilatometric and Small-Angle X-Ray Scattering Study of the Electrochemical Activation of Mesophase Pitch-Derived Carbon in Non-Aqueous Electrolyte Solution. *Carbon* **2010**, *48*, 1880–1888.

(38) Zhang, C.; Xie, Y.; Sun, G.; Pentecost, A.; Wang, J.; Qiao, W.; Ling, L.; Long, D.; Gogotsi, Y. Ion Intercalation into Graphitic Carbon with a Low Surface Area for High Energy Density Supercapacitors. *J. Electrochem. Soc.* **2014**, *161*, A1486–A1494.

(39) Endo, M.; Kim, Y. J.; Ohta, H.; Ishii, K.; Inoue, T.; Hayashi, T.; Nishimura, Y.; Maeda, T.; Dresselhaus, M. S. Morphology and Organic EDLC Applications of Chemically Activated AR-Resin-Based Carbons. *Carbon* **2002**, *40*, 2613–2626.

(40) Dreyer, D. R.; Park, S.; Bielawski, C. W.; Ruoff, R. S. The Chemistry of Graphene Oxide. *Chem. Soc. Rev.* **2010**, *39*, 228–240.

(41) Raymundo-Piñero, E.; Kierzek, K.; Machnikowski, J.; Béguin, F. Relationship between the Nanoporous Texture of Activated Carbons and Their Capacitance Properties in Different Electrolytes. *Carbon* **2006**, *44*, 2498–2507.

(42) Chmiola, J.; Yushin, G.; Dash, R.; Gogotsi, Y. Effect of Pore Size and Surface Area of Carbide Derived Carbons on Specific Capacitance. *J. Power Sources* **2006**, *158*, 765–772.

(43) Lota, G.; Centeno, T. A.; Frackowiak, E.; Stoeckli, F. Improvement of the Structural and Chemical Properties of a Commercial Activated Carbon for Its Application in Electrochemical Capacitors. *Electrochim. Acta* **2008**, *53*, 2210–2216.

(44) Vix-Guterl, C.; Frackowiak, E.; Jurewicz, K.; Friebe, M.; Parmentier, J.; Béguin, F. Electrochemical Energy Storage in Ordered Porous Carbon Materials. *Carbon* **2005**, *43*, 1293–1302.

(45) Ania, C. O.; Pernak, J.; Stefaniak, F.; Raymundo-Piñero, E.; Béguin, F. Polarization-Induced Distortion of Ions in the Pores of Carbon Electrodes for Electrochemical Capacitors. *Carbon* **2009**, *47*, 3158–3166.

(46) Merlet, C.; Rotenberg, B.; Madden, P. A.; Taberna, P.-L.; Simon, P.; Gogotsi, Y.; Salanne, M. On the Molecular Origin of Supercapacitance in Nanoporous Carbon Electrodes. *Nat. Mater.* **2012**, *11*, 306–310.

(47) Merlet, C.; Péan, C.; Rotenberg, B.; Madden, P. A.; Daffos, B.; Taberna, P.-L.; Simon, P.; Salanne, M. Highly Confined Ions Store Charge More Efficiently in Supercapacitors. *Nat. Commun.* **2013**, *4*, 2701.

(48) Merlet, C.; Salanne, M.; Rotenberg, B.; Madden, P. A. Influence of Solvation on the Structural and Capacitive Properties of Electrical Double Layer Capacitors. *Electrochim. Acta* **2013**, *101*, 262–271.

(49) Raccichini, R.; Varzi, A.; Passerini, S.; Scrosati, B. The Role of Graphene for Electrochemical Energy Storage. *Nat. Mater.* **2014**, *14*, 271–279.

(50) Ambrosi, A.; Chua, C. K.; Bonanni, A.; Pumera, M. Electrochemistry of Graphene and Related Materials. *Chem. Rev.* **2014**, *114*, 7150–7188.

(51) Stoller, M. D.; Ruoff, R. S. Best Practice Methods for Determining an Electrode

Material's Performance for Ultracapacitors. *Energy Environ. Sci.* **2010**, *3*, 1294–1301.

Graphical Table of Contents